Catena 162 (2018) 216–229

Contents lists available at ScienceDirect

Catena

journal homepage: www.elsevier.com/locate/catena

Four-topic correlation between flood dendrogeomorphological evidence and hydraulic parameters (the Portainé stream, Iberian Peninsula)

Ane Victoriano[a,*], Andrés Díez-Herrero[b], Mar Génova[c], Marta Guinau[a], Glòria Furdada[a], Giorgi Khazaradze[a], Jaume Calvet[a]

[a] RISKNAT Group, Geomodels Research Institute, Dpt. de Dinàmica de la Terra i de l'Oceà, Universitat de Barcelona (UB), 08028 Barcelona, Spain
[b] Geological Hazards Division, Geological Survey of Spain (IGME), 28003 Madrid, Spain
[c] Dpto. de Sistemas y Recursos Naturales, Universidad Politécnica de Madrid (UPM), 28040 Madrid, Spain

ARTICLE INFO

Keywords:
Dendrogeomorphology
Fluvial geomorphology
Hydraulic modelling
Palaeoflood
Spanish Pyrenees

ABSTRACT

Torrential floods are hazardous hydrological phenomena that produce significant economic damage worldwide. Flood reconstruction is still problematic in ungauged mountainous areas due to the lack of systematic data, so indirect techniques are required. This paper presents an integrated palaeoflood study of a Pyrenean stream that combines fluvio-torrential geomorphology, dendrogeomorphology, palaeoflood discharge estimation and flow hydraulics. The use of a total station and airborne LiDAR data allows detailed topography for geomorphological mapping and running a one-dimensional hydraulic model. Based on the height of scars on several damaged trees, we obtained palaeodischarges of 316 $m^3 s^{-1}$ and 314 $m^3 s^{-1}$ for the 2008 and 2010 floods. The hydraulic parameters were related to the geomorphic position of trees, showing a positive relation between most energetic geomorphic elements and both flow depth and velocity values. The most affected trees are located in intermediate energy geomorphic positions. Analysing variation in scar height and flow stage differences, we suggest that most reliable trees for peak discharge estimation correspond to those in areas related with fluvio-torrential processes of intermediate energy. This multidisciplinary palaeohydrological study relates flood hydrodynamics with the damage to trees and their geomorphological characteristics, focusing on the hydraulic parameters of the peak flow (depth, velocity and unit stream power), which has never been performed before. The proposed approach shows strong potential for palaeoflood analysis in ungauged mountain catchments with scarce non-systematic data.

1. Introduction

Hydrometeorological phenomena are one of the most recurrent causes of natural disasters worldwide and produce significant economic damage and fatalities every year (Gaume et al., 2009). Flood disasters have been increasing in number and the damage they cause in Europe over the last few decades (Barredo, 2007). In mountainous areas of Catalonia, NE Spain, flash floods and debris flows have severe socio-economic and geomorphologic impacts due to their sudden occurrence, torrential nature and the high sediment load involved (Portilla et al., 2010).

Flood hazard assessment is often based on conventional statistical magnitude–frequency analysis, which is difficult to apply in areas where rainfall data are scarce and which lack flow gauging stations. Palaeohydrology is a useful method in active torrential basins with non-systematic records that consists of the study of past floods, especially focusing on ancient extraordinary events, and encompasses different lines of research depending on the palaeoflood data and methodology adopted (Baker, 2008; Benito and Díez-Herrero, 2015; Lang et al., 2004; Webb and Jarrett, 2002). Extreme flood reconstruction has been carried out using a variety of data sources and evidence, such as sedimentological (Benito et al., 2003, 2015; Kochel and Baker, 1982), geomorphological (Baker et al., 1988; Baker and Pickup, 1987), dendrochronological (Ballesteros-Cánovas et al., 2016; Gottesfeld, 1996; Kundzewicz et al., 2014; Malik and Matyja, 2008; Sigafoos, 1964; Yanosky and Jarrett, 2002; Zielonka et al., 2008), and lichenometric (Gob et al., 2003) indicators.

Many authors have reconstructed palaeofloods using dendrogeomorphology. This provides information on past events recorded in flood dendrogeomorphological evidence (FDE) in riverbed and riverbank trees (for reviews see: Ballesteros-Cánovas et al., 2015b; Benito and Díez-Herrero, 2015), and also hydraulic parameters like flow

* Corresponding author.
E-mail addresses: ane.victoriano@ub.edu (A. Victoriano), andres.diez@igme.es (A. Díez-Herrero), mar.genova@upm.es (M. Génova), mguinau@ub.edu (M. Guinau), gloria.furdada@ub.edu (G. Furdada), gkhazar@ub.edu (G. Khazaradze), jcalvet@ub.edu (J. Calvet).

https://doi.org/10.1016/j.catena.2017.11.009
Received 25 January 2017; Received in revised form 19 October 2017; Accepted 3 November 2017
Available online 12 November 2017
0341-8162/

velocity, depth and power, by means of hydrodynamic modelling (Ballesteros-Cánovas et al., 2010, 2015a). Numerous studies relate flood discharges with flow hydraulics using different empirical equations (Bagnold, 1980; Chanson, 2004; Chow, 1959; Costa, 1983; Ferguson, 2005). Other work deals with flow hydraulics and fluvial geomorphology from different perspectives: flood geomorphology (Baker et al., 1988), the stability of geomorphological elements (Nicholas and Walling, 1997; Ortega and Garzón, 1997) or past flood discharges and deposits (Baker, 1987; Kochel and Baker, 1982; Sánchez-Moya and Sopeña, 2015). However, FDEs have rarely been associated with the geomorphic position of the trees (Ruiz-Villanueva et al., 2010) or other local characteristics of the river reach (Ballesteros-Cánovas et al., 2016).

However, these methods tend to be limited in mountains areas. Dendrogeomorphological studies are conditioned by the number of trees in the study area, which in some cases is small. High-resolution geomorphological mapping is difficult to carry out in remote areas. Palaeodischarge reconstruction in ungauged catchments requires adequate topographic data for hydraulic modelling, which are usually scarce in forested mountain areas. Regarding flow hydrodynamics, the calculation of hydraulic parameters depends on the estimated peak discharge.

This paper reconstructs flood events by combining all these disciplines (Fig. 1) and its aim is to quantify the relation between flood hydrodynamics and the geomorphological characteristics of damaged trees. Flow hydraulics is analysed according to the specific geomorphic position of trees and the stream power obtained from hydraulic modelling is used to estimate the mobilizable particle size, which is compared to measurements taken in the field to assess its reliability. Such multidisciplinary analysis especially focusing on hydraulic parameters has never been carried out before in a selected study area, and allows us to improve our knowledge of fluvio-torrential dynamics in areas where few source data are available.

2. Problematic study area and hazard

The multidisciplinary approach presented in this paper was performed in the 5.72 km^2 Portainé drainage basin (in the county of Pallars Sobirà, Catalonia, Spain), located in the Eastern Pyrenees (Fig. 2a). The maximum altitude is 2439 m a.s.l. (Torreta de l'Orri). Two main streams drain the basin towards the north, the Portainé stream (5.7 km long) and its tributary the Reguerals stream (3 km long). Their confluence is at 1285 m a.s.l. and then the Portainé stream flows until its confluence with the Romadriu River (part of the Ebro River Basin) at 950 m a.s.l. (Fig. 2c). An access road to the Port-Ainé ski station crosses both streams at various points. The climate is alpine Mediterranean, with a mean annual rainfall of 800 mm and 5 °C–7 °C mean annual temperature (Meteocat, 2008).

From a geological perspective, the Portainé basin is located in the Pyrenean Axial Zone (Fig. 2b). In the study area, the bedrock is composed of highly folded and fractured Cambro-Ordovician metapelites and sandstones with quartzite intercalations. Thick surficial colluvial materials irregularly cover large parts of the terrain. Due to the highly fractured bedrock and the unconsolidated surficial deposits, materials are easily eroded and mobilized along the streams. Geomorphologically, the catchment can be divided in two sectors (IGC, 2013). The southern part corresponds to the headwaters and consists of lower gradients (less than 25° and commonly around 10°–20°) and a poorly entrenched drainage network. The northern sector has higher gradients (> 25°) and heavily entrenched streams (Fig. 2c).

The Portainé and the Reguerals streams are characterized by a high level of torrential activity especially since 2006, with debris flood, hyperconcentrated flow and/or debris flow events producing significant damage to infrastructure, mainly where the road crosses the streams. From 2006 to 2015, ten events occurred in this area (IGC, 2013; Palau et al., 2017), even without extraordinary rainfall values. In addition, dendrogeomorphological studies have proved the occurrence of previous torrential events, although their frequency was much lower (Furdada et al., 2016; García-Oteyza et al., 2015). In order to reduce the impact of these events, 15 sediment retention barriers have been installed along the channels since 2009 as a hydrological correction measure (Luis-Fonseca et al., 2011). However, the problem remains and the increasingly entrenched streams show a significant erosive tendency (Victoriano et al., 2016).

Our specific study area corresponds to the most downstream 500 m long reach of the Portainé stream. At the confluence with the Romadriu River, an elongated alluvial debris cone has formed, mainly composed of sub-rounded to sub-angular decimetric boulders. High sediment load torrential events change the morphology of the mobile riverbed easily, and also affect the riverbank trees. In general, the vegetation in the area constitutes a deciduous broadleaf forest with a variety of species.

3. Material and methods

The methodological approach adopted for this study is summarized in Fig. 3, which shows each research topic and the integration of the methods to obtain the final results.

3.1. Geomorphological mapping and analysis

Detailed geomorphological studies and mapping of the features was carried out. This analysis consisted of two steps: (i) topographic and geomorphological fieldwork, and (ii) GIS mapping.

Detailed topographic data were acquired in March 2014 using a Leica TC 1700 total station. This taquimetric survey focused on localizing trees and defining abrupt topographic changes (breaklines), in order to assemble a complete point dataset (Keim et al., 1999) consisting of 1118 points (853 ground points and 265 tree points) in a 4850 m^2 area. In addition, in places where trees showing external FDE were identified, we also obtained detailed topographic cross sections. Differential RTK GNSS methods were carried out to accurately measure

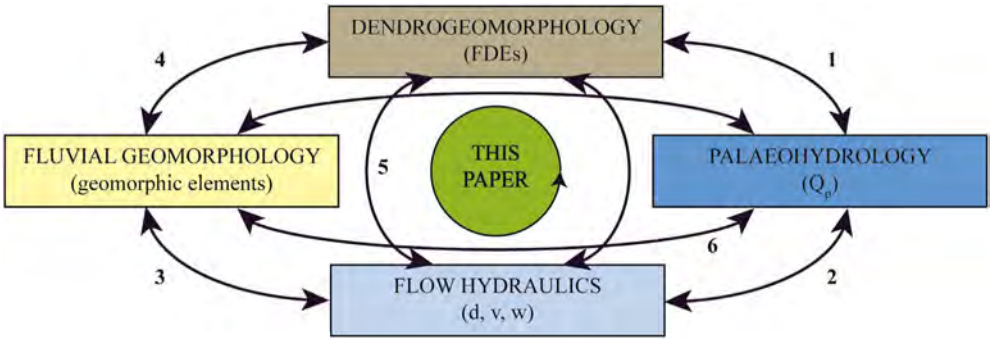

Fig. 1. Conceptual diagram of the disciplines and methods combined in the present study. Numbers indicate some of the groups of existing studies relating different research topics. 1: Dendrogeomorphology *vs* palaeohydrology (for reviews see: Ballesteros-Cánovas et al., 2015b; Benito and Díez-Herrero, 2015). 2: Palaeohydrology *vs* flow hydraulics (Bagnold, 1980; Chanson, 2004; Chow, 1959; Costa, 1983; Ferguson, 2005). 3: Flow hydraulics *vs* fluvial geomorphology (Nicholas and Walling, 1997; Ortega and Garzón, 1997; Sánchez-Moya and Sopeña, 2015). 4: Fluvial geomorphology *vs* dendrogeomorphology (Ballesteros-Cánovas et al., 2016; Ruiz-Villanueva et al., 2010). 5: Dendrogeomorphology *vs* flow hydraulics (Ballesteros-Cánovas et al., 2010, 2015a). 6: Palaeohydrology *vs* fluvial geomorphology (Baker, 1987; Baker et al., 1988; Kochel and Baker, 1982).

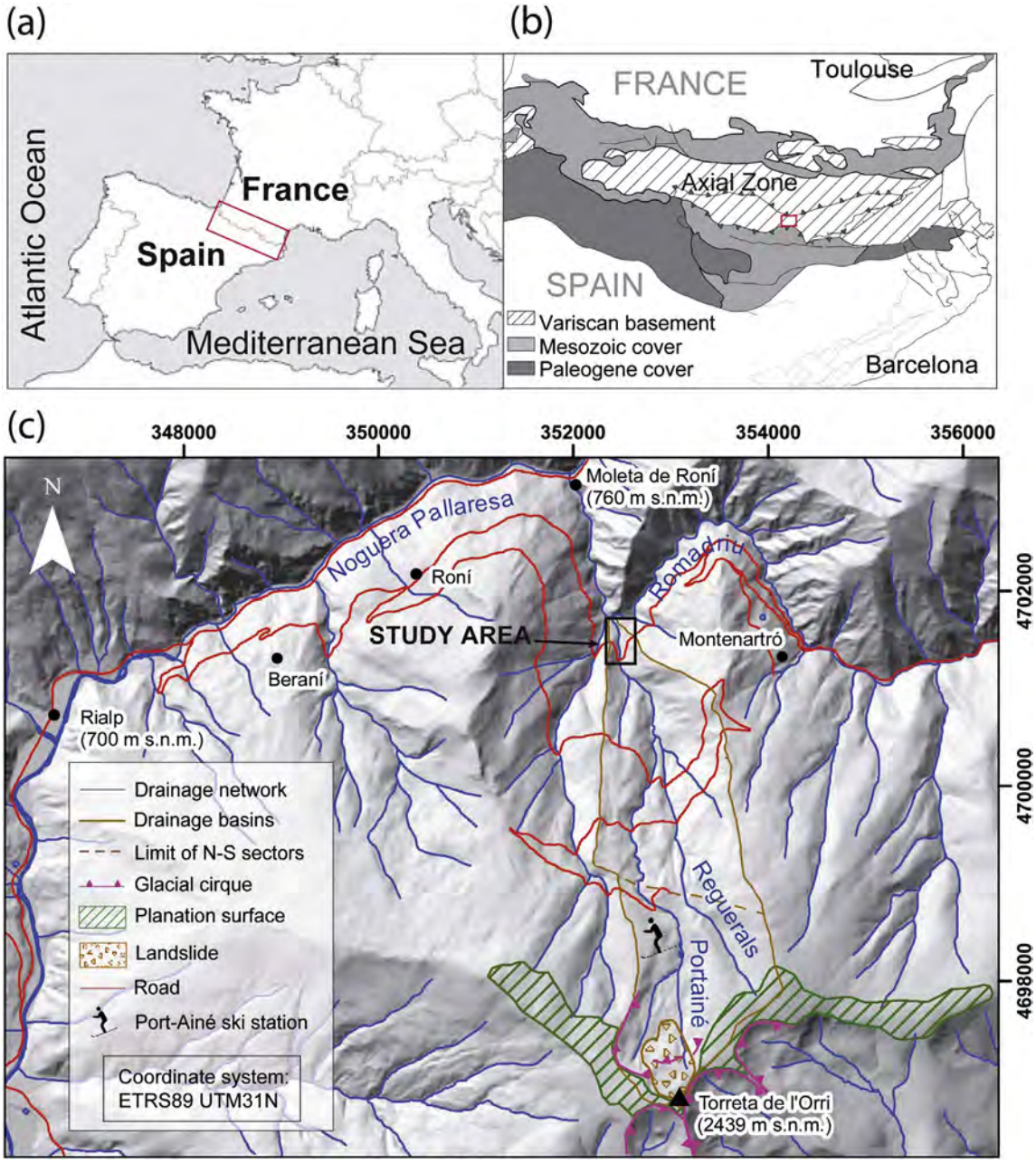

Fig. 2. (a) Geographic setting, with the Pyrenees marked with a red square. (b) Geological setting of the study area, located in the Axial Pyrenees, and the area in (c) marked with a red square. (c) Geomorphological context of the Portainé basin and the specific study area marked with a black square, corresponding to the most downstream reach. (For interpretation of the references to colour in this figure legend, the reader is referred to the web version of this article.)

the absolute coordinates of certain control points (Khazaradze et al., 2016) used to georeference the dense measurements obtained with the total station. During the topographic field survey, the main geomorphological elements were identified following the proposal of Church et al. (2012) and their limits were measured with the total station. The geomorphological elements and deposits were roughly classified as: functional channel, distributary channels of the cone, gravels and boulders. In addition, alluvial terraces were identified, as well as other features like levees, escarpments and flow paths. During subsequent field surveys in March 2015, September 2015 and June 2016, morphological changes in landforms, elements and facets (different parts of the elements) were identified; they mainly occurred along the channels and did not alter the position of riverbed and riverbank trees.

The deposits and forms were mapped using the ArcGIS 10.2.2 software (ESRI, 2014), creating a detailed geomorphological map.

3.2. Dendrogeomorphological analysis

Dendrogeomorphology uses palaeohydrological data sources to provide information on past torrential events recorded in trunks, branches and roots of riverbed and riverbank trees (Díez-Herrero, 2015). Tree-ring analysis has been widely applied in the study of floods (for reviews, see: Ballesteros-Cánovas et al., 2015b; Benito and Díez-Herrero, 2015). The dendrogeomorphological study carried out in Portainé was divided in three complementary tasks: (i) dendrochronological sampling, (ii) tree-ring analysis and the corresponding FDE dating, and (iii) geomorphological analysis of tree positions.

Dendrochronological sampling was carried out in March 2014, March 2015 and September 2015, using a strategy based on recognition in the field of external disturbances. The trees selected were those showing the most probable evidence of having received the impact of

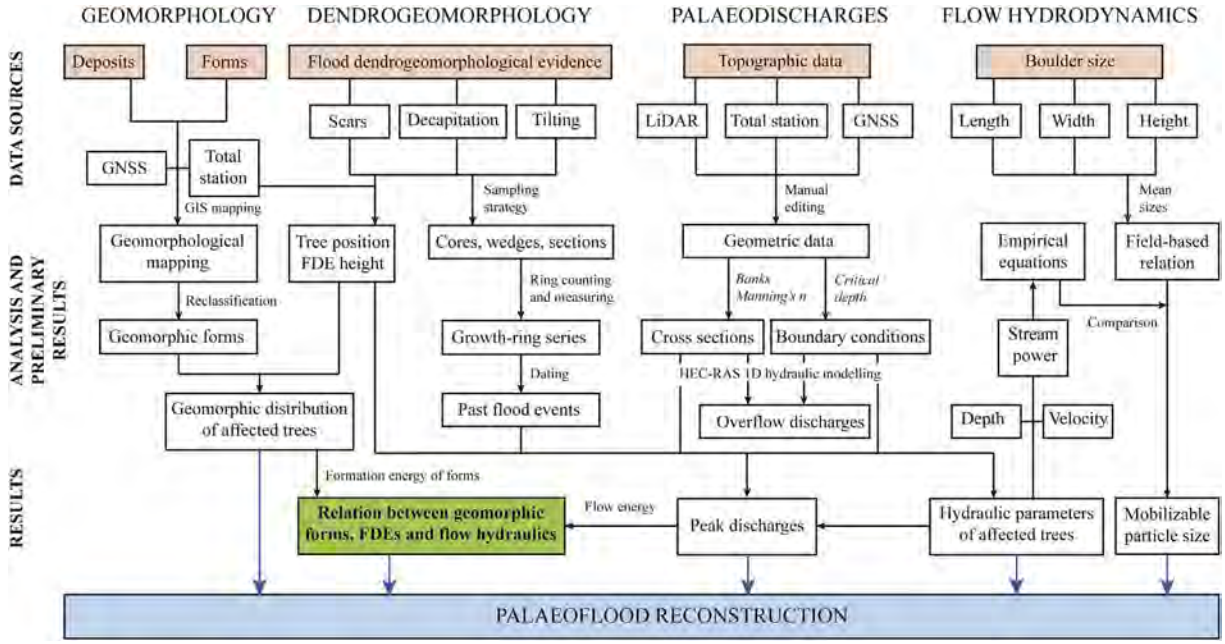

Fig. 3. Flow diagram showing the multidisciplinary methodology applied in this study for palaeoflood reconstruction, from data sources to results, following four main disciplines: geomorphology, dendrogeomorphology, palaeodischarge estimation and flow hydrodynamics.

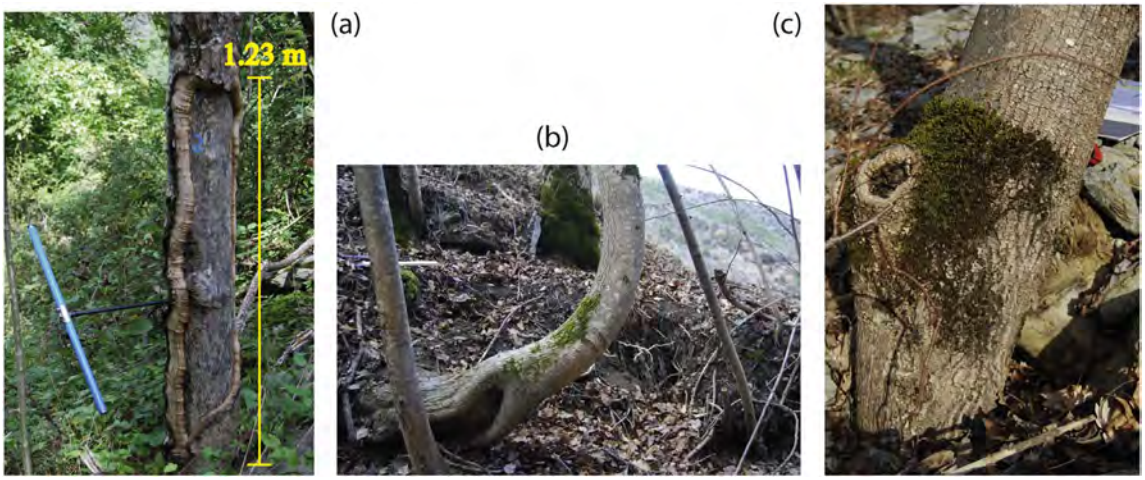

Fig. 4. External damage on trees located on the riverbanks of the Portainé stream. (a) Scar formed in 2008. (b) Stem tilting. (c) Decapitated tree.

boulders and/or large pieces of wood transported by the flow: mainly injured, decapitated and tilted trees (Fig. 4), but also a few trees with exposed roots. The trees were sampled following accepted dendrogeomorphological procedures (Stoffel and Bollschweiler, 2008; Díez-Herrero et al., 2013; Stoffel and Corona, 2014). The geographic position of each tree was measured using a total station, and the heights of scars and decapitation nodes were also recorded. Additional information collected included an identifier code, the sampling date, species, a description of the tree (height and perimeter), a description of the FDE (type, height and size), a description of the sample (height) and photos of the tree. Cylindrical samples (cores) were obtained using a Pressler increment borer of 5 mm diameter. Some wedges were also extracted from overgrowing callus in scarred trees and cross sections were cut in some death trees. We analysed 57 trees from 9 different species (151 samples) providing a multievidence population of *Populus tremula* L. (common aspen), *Populus nigra* L. (black poplar), *Fraxinus excelsior* L. (ash), *Prunus avium* L. (wild cherry), *Quercus petraea* (Matt.) Liebl. (sessile oak), *Tilia platyphyllos* Scop. (large leaf linden), *Juglans regia* L. (common walnut), *Acer campestre* L. (field maple) and *Salix caprea* L. (goat willow).

In this study, we only considered external evidence on trees. In the laboratory, tree-ring analysis of cores, wedges and sections (Génova et al., 2015) consisted of: (i) air-drying, cutting or sanding samples; (ii) measuring tree-ring width using a LINTAB table (with 1/100 mm accuracy) and the associated software TSAPWin (RinnTech, 2003); (iii) cross-dating using visual and statistical techniques (Cook and Kairiukstis, 1990); and (iv) quality checking using the Cofecha software (Grissino-Mayer, 2001). This process allowed us to date scars in tree-ring series and consequently, torrential events. The last ring of dead trees was dated by comparing tree-ring series with living trees of the same species. For palaeoflood reconstruction, the scar formation years (dated following the procedure described) and their height (measured in the field) were used. Additionally, we considered the location of decapitated trees, tilted trees and exposed roots for the geomorphic analysis. This information was compiled within a dendrogeochronological database.

The inclusion of the dendrogeochronological database in a GIS environment, using ArcGIS 10.2.2 software (ESRI, 2014), allowed us to

study the geomorphological setting of disturbed trees. Based on the geomorphological mapping and tree positions, geomorphic features were reclassified according to their formation energy (Ruiz-Villanueva et al., 2010). This led to a considerably more elaborate classification of the geomorphic forms, elements and facets. Moreover, the detailed geomorphic position of each tree was determined in the field, and the trees were classified according to the geomorphic form (*e.g.* riverbed), element (*e.g.* gravel bar) or facet (*e.g.* bar tail) in which they were located. This provided us with the spatial distribution of FDEs according to the formation energy of the geomorphic form on which they were located. Other geomorphological characteristics (*e.g.* channel reach morphology and tree exposure to the flow) were not considered in this study because they were the same for all the scarred trees (a straight channel and exposed trees). Therefore, the geomorphic position according to geomorphic units was the best evidence available to relate flow hydrodynamics and FDE formation.

3.3. Palaeodischarge estimations and hydraulic modelling

Palaeofloods were reconstructed using the one-dimensional hydraulic simulation software HEC-RAS 4.0 from the US Army Corps of Engineers (USACE, 2008). This model was used to obtain palaeoflood discharges and other hydraulic parameters such as stage, water depth, velocity and stream power. A 1D model was run instead of a 2D model due to the following groups of factors: a) geometric channel characteristics (a lack of high-resolution and high-accuracy 2D topographic data; detailed cross-sections coinciding with tree locations measured with total station; narrow valley with length/width ratio > 3:1; and a lack of anthropic features, such as bridges or culverts, along the channel); b) hydrodynamic factors (unidirectional flow patterns during floods; limited secondary transversal flows due to the narrowness of the valley and the steep gradient with waterfalls and rapids); and c) other evidence (scar height–riverbed parallelism suggesting a sub-uniform to gradually variable flow). The parameters and conditions required to run the hydraulic model were: (i) geometric data, (ii) boundary conditions, and (iii) discharges.

Regarding the geometric data, HEC-RAS works with transversal cross sections (XS sections). Topographic data from two different sources were available for the study area: total station and airborne LiDAR (light detection and ranging) data. Total station data were acquired in the field (see Section 3.1.) and provided a high degree of accuracy but with a slightly low point density. LiDAR data were collected from a Cessna Caravan 208B aircraft using a Leica ALS50-II topographic LiDAR sensor, owned by the Cartographic and Geological Institute of Catalonia (ICGC), and the point cloud was georeferenced and filtered using TerraScan software (Terrasolid, 2016). The capacity of LiDAR data to create high-resolution elevation models is widely accepted (Tarolli, 2014). However, in our mountain study area with steep slopes and dense vegetation, the LiDAR dataset provided good coverage but had a low degree of elevation accuracy (about 50 cm RMSE) and did not produce very high-resolution topography (0.63 ground point/m^2). Taking into account the strengths and limitations of the data sources, two hydraulic models were run with different geometric data. For the first one, the cross sections measured with the total station in the field (23 XS sections) were manually introduced. For the second one, we combined both sets of topographic data. The LiDAR points were added into the total station dataset and carefully analysed in order to assess their suitability. Some adjacent points showed significant differences in elevation, which were attributed to: (i) small but detectable erosion and accumulation between the 2011 LiDAR and 2014 total station data; and (ii) the actual morphology of the steep terrain (*e.g.* stream entrenchment, escarpments and steep slopes). In order to overcome these limitations, the points were manually edited using objective criteria of congruence and acceptability, consisting of detecting erroneous points by comparing their coordinates with the surrounding points. This was carried out by creating 0.5 m (in steep areas) or 1 m (in flat areas) buffers for total station points and intersecting these with the LiDAR ground points. Establishing a maximum tolerance threshold of 0.5 m for the differences in elevation between the two topographic data sources, incoherent LiDAR points were deleted. Finally, a bare-earth Digital Elevation Model (DEM), represented by a triangulated irregular network (TIN), was created with the selected terrain points and sections were extracted from it (35 XS sections), using the HEC-GeoRAS 10.2 extension (USACE, 2012) for ArcGIS. The advantage of the TIN-based model is that it allowed us to input additional transversal profiles; but its weakness is that the LiDAR data can distort and smooth the detailed sharp topography obtained in the field. In addition, the stream centreline, banks and levees were added. The limits of the riverbanks were defined as coinciding with roughness changes, so that a Manning's n value for the left bank, channel and right bank was established for each cross section. The roughness coefficient was obtained from field observations, based on the method in Arcement and Schneider (1989).

The boundary condition upstream and downstream from the modelled reach was critical depth, because both boundary sections correspond to small waterfalls (> 2 m high) in a stable bedrock riverbed, identified in the field. These are hydraulic jumps with a critical flow (Froude number = 1), especially during flood events, so they are suitable for the critical-depth method (Bodoque et al., 2011). The model was run as a steady flow, as the input was peak discharge values, and the flow regime modelled as supercritical.

Palaeodischarges were calculated using external scars as palaeostage indicators (PSIs). This evidence provides the most precise information on both the date and the magnitude of the event, as they allow us to determine both the precise year in which they were formed, by dendrochronological dating, and the minimum water depth of the flow by measuring the height of the scar and/or its absolute altitude. In our study, we dated external scars from events in 2000 (4 scars), 2006 (1 scar), 2008 (19 scars) and 2010 (6 scars). The scars from 2000 were almost closed and did not provide information on the water stage. In 2006 just one tree was scarred, so it was not considered enough evidence as a PSI. Therefore, only the 2008 and 2010 events could be reconstructed, as they provided a representative number of scars and their height could be reliably measured in the field; but they are also the latest and most destructive events documented. Although two events occurred in 2008 (September and November) and two others in 2010 (July and August), we assume that the scars were formed by a single event in each year. The scars from 2008 all appear to have been formed in the high-magnitude torrential flood that occurred in September, which produced documented damage to a bridge located just upstream of the study reach (IGC, 2013). In contrast, the lower-magnitude event that occurred in November did not have any effect at that point. The event in July 2010 did not transport material along the study reach, because it accumulated in sediment retention barriers that had recently been emplaced (IGC, 2010b); so, the 2010 scars would correspond to the August event, when the barriers were fully loaded and the flow transported a large amount of sediment. We selected the trees showing scars that corresponded to those event years (25 trees). For each year, we carried out a normality test of height differences (d in Eq. (3)) in order to detect outliers, comparing the samples with a Gaussian distribution. This process allowed us to detect an anomalous scar from 2008, which did indeed show an odd shape in the field. Since its origin may not therefore have been torrential, it was deleted before we simulated the discharge values. So, 18 scars (6 *P. tremula*, 6 *P. nigra*, 2 *F. excelsior*, 2 *P. avium*, 1 *Q. petraea* and 1 *A. campestre*) were considered for the 2008 modelling (9 of them dated from wedges) and 6 scars (2 *P. tremula*, 2 *F. excelsior*, 1 *Q. oetraea* and 1 *T. platyphyllos*) for 2010 (1 dated from a wedge). Peak discharges were calculated for the palaeofloods analysed using the step-backwater method (Ballesteros-Cánovas et al., 2010; O'Connor and Webb, 1988), by inputting increasing peak discharge values into the model and finding the best fit of water surface elevation with the height of the scars. Thus, for each event and each geometric dataset introduced (XS section), the trial-and-

error technique was used to estimate the peak discharge (with a precision of 1 $m^3 s^{-1}$), by finding the value that showed the minimum mean absolute error (σ or MAE) and mean squared error (MSE) in the heights (difference between scar height and modelled water stage), defined as:

$$\sigma = \frac{\sum_i^n d_i}{n} \quad (1)$$

$$\mathrm{MSE} = \frac{\sum_i^n d_i^2}{n} \quad (2)$$

where n is the number of scars and d is the absolute value of the difference between the height of the scar and the water stage, estimated by the expression:

$$d = |Z_{FDE} - Z_Q| \quad (3)$$

where Z_{FDE} is the altitude of the scar in meters (m) and Z_Q is the water surface elevation for the modelled peak discharge in meters (m), both measured in the cross section where the scar is located.

Finally, the peak discharges were calculated as the weighted arithmetic mean of the discharges obtained from the two geometric datasets, as:

$$Q_{2008} = \frac{\left(\frac{1}{\sigma_{TIN}^2} Q_{TIN}\right) + \left(\frac{1}{\sigma_{TE}^2} Q_{TS}\right)}{\frac{1}{\sigma_{TIN}^2} + \frac{1}{\sigma_{TS}^2}} \quad (4)$$

where σ_{TIN} and σ_{TS} are the absolute error of the TIN-based model and the one with the total station data respectively, and Q_{TIN} and Q_{TS} are the estimated peak discharges in $m^3 s^{-1}$.

As flow in an alluvial cone can be difficult to simulate using a 1D model, we also calculated the minimum peak discharge for bank overflow. This is the threshold for cone flooding and consequently marks a change in the distribution of the flow discharge. This critical overflow discharge was obtained from the cross section located at cone apex.

3.4. Flow hydrodynamics

We extracted other hydraulic parameters from the HEC-RAS results for each cross section, such as water depth, velocity and total stream power. These parameters were then obtained for the specific position of each scarred tree used in the hydrodynamic modelling. Depth was calculated by subtracting the elevation of the base of the tree from the water surface elevation. For velocity, we considered the value for the part of the cross section in which the tree was located (left bank, channel or right bank). The unit stream power was obtained by dividing the total stream power obtained by the active width of the flow at each part of the cross section.

Knowledge of the flow hydraulics allowed us to estimate, by means of empirical equations, the particle size that might be mobilized by the flow. These calculations were carried out for the 2008 event and in the deposit of the alluvial cone, as discharge estimation was more reliable and accurate for 2008 than for the 2010 event. In the field, we also measured the maximum (length), medium (width) and minimum (height) axes of a representative population of boulders deposited in the alluvial cone, which allowed us to compare the results obtained from empirical calculations with actual deposited material. The diameter of the transported boulders was calculated using different empirical equations. The mobilizable particle size is a function of the critical unit stream power, so the hydraulic parameters needed for these equations were obtained from the upstream cross section of the alluvial cone as the flow in the study site was supercritical. The three relations applied were:

$$\omega_c = a \cdot D^b \quad (5)$$

where ω_c is the critical unit stream power in W/m^2, a and b are numerical constants that depend on the source (Costa, 1983; Gob et al., 2003; Jacob, 2003; Williams, 1983), and D is the particle diameter in millimetres (mm);

$$\omega_c = c_1 \cdot D^{1.5} \cdot \log_{10}\left(\frac{c_2 \cdot d}{D}\right) \quad (6)$$

where d is the water depth and c_1 and c_2 are numerical constants again determined by different authors (Bagnold, 1980; Ferguson, 2005), and;

$$C_d = \left(\frac{0.6}{\left(\frac{d}{H}\right)\left(\frac{L}{B}\right)}\right) + 0.9 \quad (7)$$

where C_d is the drag coefficient, assumed to be 0.95, and H, B and L are the distances (diameters) corresponding to the main three main axes of the particles: height (minimum), width (intermediate) and length (maximum), respectively (Carling et al., 2002). In fact, this equation assumes the morphometry of the particle is dependent on the water depth; and propose that the mobilized boulders should be considered as relation of the three axes, which depends on several factors, such as the lithology, internal structure and fractures of the material.

4. Results

4.1. Geomorphological mapping and geomorphic forms

A geomorphological map of the torrential system was obtained based on the March 2014 topography. Multi-temporal field campaigns (2014–2016) showed that the distribution and morphology of the geomorphological elements and deposits changed over time, especially those associated with the riverbed, and therefore the Portainé stream is very dynamic. These changes are mostly visible in the functional channel and at the lowest level of alluvial terraces. In general, the stream shows an erosive tendency, which is reflected in the backward motion of the bank escarpments that delimit the channel. In the alluvial cone area, the flow tends to deposit boulders transported during debris flow and flood events.

13 types of geomorphic forms, elements and facets were identified and mapped, which are ordered according to their formation energy as: in-channel (functional active channel), gravel bars, terrace 1 (low terrace), terrace 2 (high terrace), natural levee, main inactive channel of cone, secondary inactive channels of cone, upper deposits of cone, middle deposits of cone, lower deposits of cone, artificial levee (dyke), left-side slope and right-side slope (Table 1 and Fig. 5).

Table 1
Geomorphic position of the trees analysed and dated by dendrochronological techniques and the number of trees with external scars used for hydrodynamic modelling of the2008 and 2010 events.

Geomorphic form		Trees with FDE	Scarred trees
Riverbed	In-channel	1	1
	Gravel bar	1	1
Alluvial terraces	Terrace 1	4	3
	Terrace 2	5	4
Levees	Natural levee	0	0
	Artificial levee	5	1
Alluvial cone	Main channel	3	0
	Secondary channel	3	2
	Upper deposits	14	1
	Middle deposits	8	6
	Lower deposits	5	2
Slope	Left side	4	0
	Right side	4	3

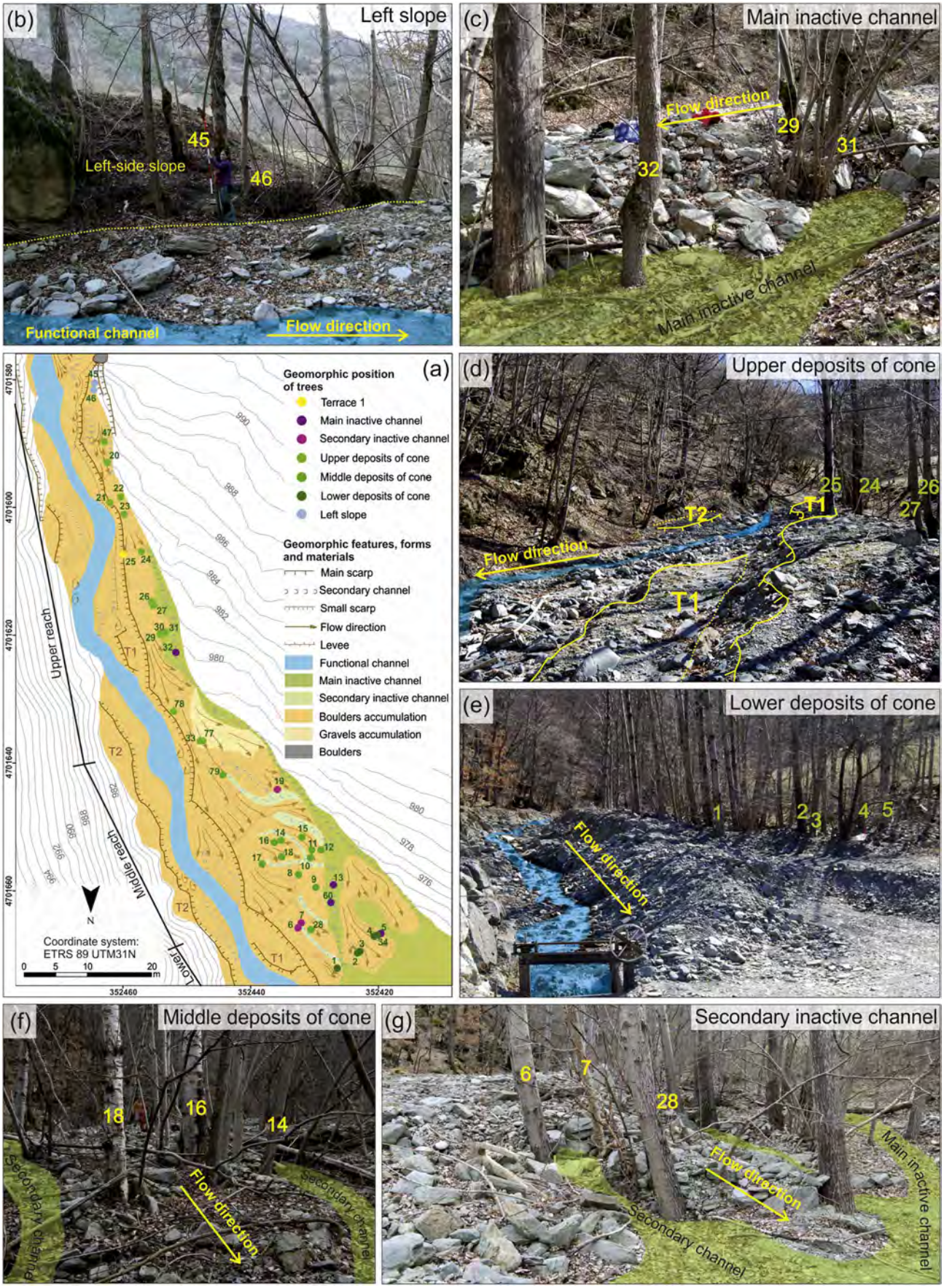

Fig. 5. (a) Detailed geomorphological mapping (September 2015) of the alluvial cone showing the main geomorphological features, forms, deposits and the position of the trees that were sampled for the dendrogeomorphological analysis; where trees are coloured according to geomorphic position. (b), (c), (d), (e), (f), (g) Pictures showing examples of different geomorphic positions identified in the study area. (For interpretation of the references to colour in this figure legend, the reader is referred to the web version of this article.)

Table 2
Estimation of peak flood discharges using hydraulic modelling based on scars as dendrogeomorphological palaeostage indicators.

Year	Geometric data source	Peak discharge, Q_p ($m^3 s^{-1}$)	Absolute error, σ (m)	Mean squared error, MSE (m)	Variance (m)
2008	TIN	300	0.35	0.23	0.11
	Total station	321	0.21	0.08	0.04
2010	TIN	314	0.7	0.35	0.04
	Total station	–	–	–	–

4.2. Dendrogeomorphological evidence

Regarding external disturbances, we identified 10 decapitations, 41 external scars, 25 tilted trees and 3 trees with exposed roots.

Determination of the geomorphic position of the trees allowed us to relate the spatial distribution of FDE along the torrent with the geomorphological elements (Fig. 5). Table 1 shows the geomorphic position of all the trees analysed and of the scarred trees used for hydraulic modelling. The trees analysed are located at 12 different geomorphic forms; indeed, at all of the identified forms except for natural levees. Most of them are located in the alluvial cone (58%), alluvial terraces (16%) and slopes (14%).

4.3. Flood discharges

The peak discharges obtained for 2008 and 2010 are presented in Table 2. For each case, the value that minimized both absolute and mean squared error was considered. For 2008, the calculated discharges were 300 $m^3 s^{-1}$ from the TIN topography (Fig. 6) and 321 $m^3 s^{-1}$ from the total station topography. These results were weighted according to their errors (Eq. (4)), to give a peak discharge of 316 $m^3 s^{-1}$ (σ = 0.18 m). Given that for 2010 there were only 4 scars corresponding to cross sections measured with total station, the 314 $m^3 s^{-1}$ discharge (σ = 0.7 m) obtained from the TIN-based model was considered as the more reliable peak discharge value.

For the critical overflow discharge, we obtained a 43 $m^3 s^{-1}$ value for initial overbank flow and formation of crevasse splays, named partial overbank discharge. However, the complete flooding of the cone does not occur until the flow exceeds the total critical overbank discharge, estimated to be 58 $m^3 s^{-1}$. Therefore, higher peak discharges produce the inundation of the debris cone. These are considered extraordinary events, like those in 2008 and 2010.

4.4. Hydraulic parameters and mobilized particle size

Considering the discharge values obtained for the 2008 and 2010 events, the flow hydraulics was similar in both cases. Fig. 7 shows the flooded area and the water depth in the most downstream part of the study area for the 2008 event. That episode almost totally flooded the alluvial cone, generating scars on trees due to the impact of boulders and large pieces of floating wood.

The hydraulic parameters obtained from our hydrodynamic modelling were water depth (d), flow velocity (v) and unit stream power (ω) for the left bank, channel, and right bank of each cross section (see results in Supplementary material Table 1). *In situ* hydraulic parameters for the specific position of each scarred tree are shown in Table 3.

For the empirical equations for particle size estimation, the water depth and unit stream power values were those corresponding to left bank of the section at the apex of the cone (section U-Uc′), for the 2008 peak discharge. These values were 1.03 m and 5221.92 Nm^{-2}. The boulder size mobilized by the flow and deposited in the cone was also obtained from the measurements of the three axes (Table 4). This allowed us to establish the following field-based diameter relationships: $B = 0.74\,L$, where B is width and L length; and $H = 0.43\,L$, H being height. Table 5 gives the particle diameters calculated for the Portainé alluvial cone, considering the relations proposed by different authors.

4.5. Relation between geomorphic forms, FDE and flow hydraulics

All the aspects analysed in the previous sections were linked together to obtain more complete knowledge of the hydrodynamics of the Portainé stream, the behaviour of the riverbank trees and the morphology of the area.

The formation of dendrogeomorphological disturbances depends on the geomorphic position of the trees. 103 disturbances (decapitations, scars, stem tilting and root exposure) in 12 geomorphic positions were analysed in our study area from 57 different trees. The number of pieces of evidence per tree (total number of FDE / number of trees) was calculated for each geomorphic form, and is shown in Fig. 8 (see results in Supplementary material Table 2). There were few instances of FDE in the riverbed trees (in-channel and gravel bars), despite these being the most energetic positions. This is due to the low numbers of trees in these geomorphic positions and therefore few samples for dendrochronological analysis. Most FDE was located in the alluvial cone, both in the main or secondary inactive channels (2.7 FDE per tree) or in the deposit area (2 FDE per tree). Therefore, in the Portainé study area, the most intensely damaged trees are concentrated on the geomorphological elements related to processes of intermediate energy (second terrace and alluvial cone).

The geomorphological features of the valley bottom are also related to flow hydraulics, and in this specific case, the stability of geomorphic forms associated with torrential processes depends on the energy of the water. The hydrodynamic modelling allowed us to determine the specific velocity and water depth values for the scarred trees. These hydraulic parameters were then associated with the geomorphic element in which each tree was located. Fig. 9 represents the relation between the energy of flow, affectation of trees and geomorphology. Higher velocity and depth values indicate areas where torrential processes are more intense, and therefore correspond to energetic geomorphic forms.

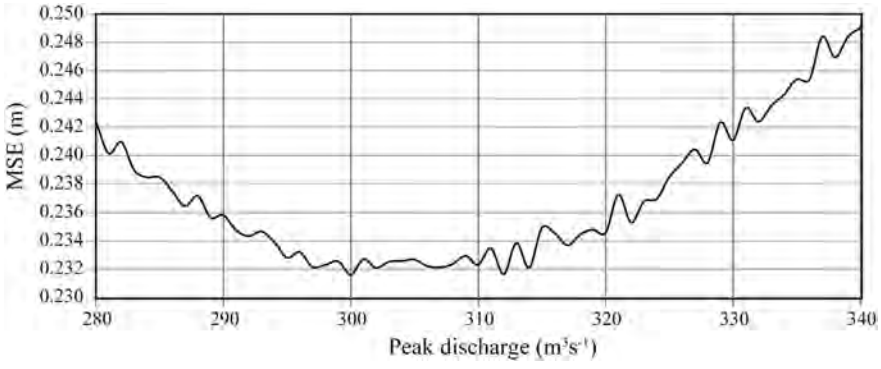

Fig. 6. Peak discharge estimation for 2008 from the TIN-based hydraulic modelling. The accepted value corresponds to the minimum mean squared error obtained from the average of the squared errors of 18 tree scars.

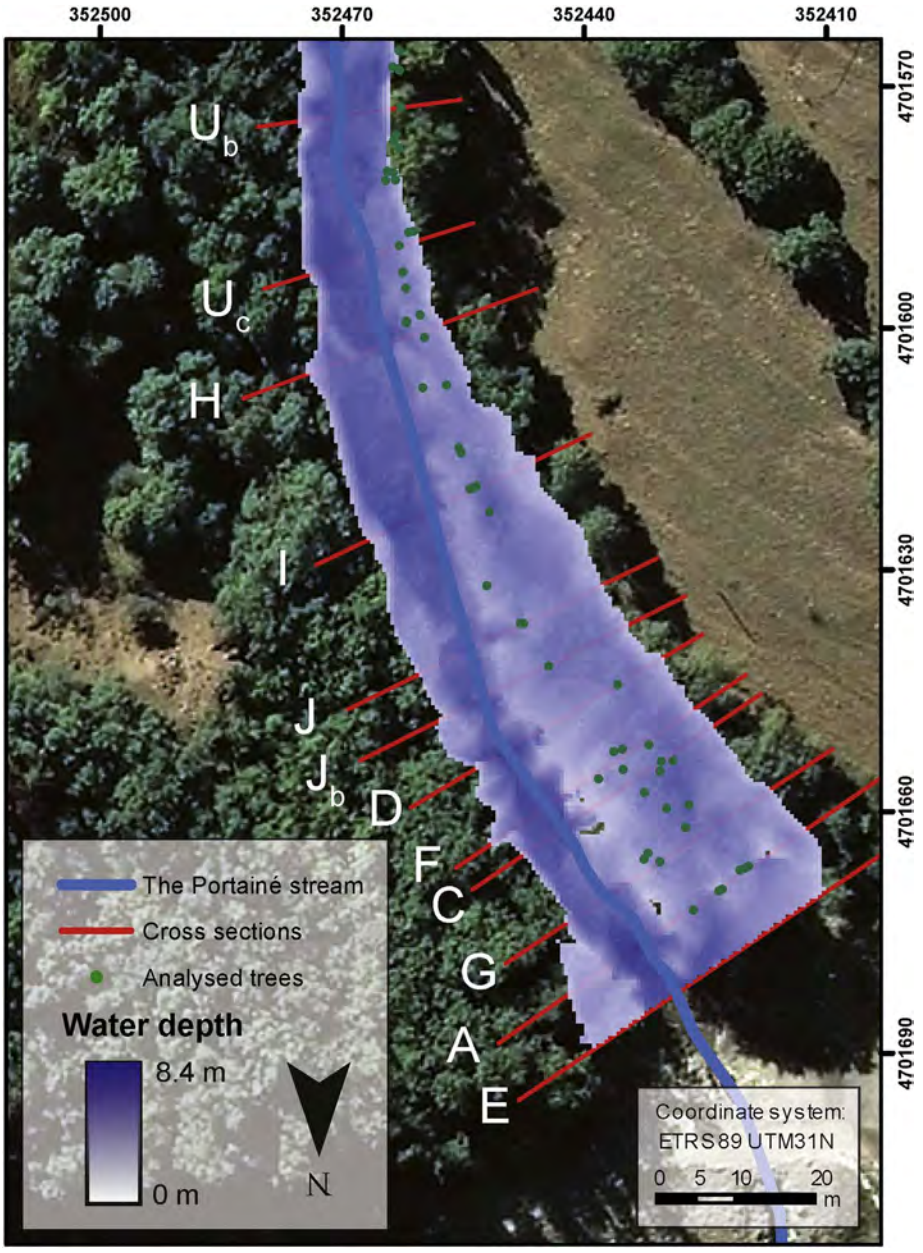

Fig. 7. Bathymetric map of the area flooded in the 2008 event, corresponding to the alluvial cone.

These most energetic geomorphological elements are close to the riverbed (in-channel and gravel bars). Far from the riverbed, there is a decrease in the flow energy, in terms of both hydraulic parameters and the intensity of the torrential processes related to the geomorphic features (Fig. 9). In addition, the largest number of scars was observed in the alluvial cone, which corresponds to torrential processes of intermediate intensity. Taking into account that every scarred tree in the study area was sampled, the number of samples does not condition the concentration of scars in the alluvial cone and it represents the geomorphic form where most trees are affected during torrential events.

The relation of scars, geomorphic forms and flow hydrodynamics can be assessed by comparing the differences between scar height and the modelled water stage (Eq. (3)) of the trees, according to their geomorphic position. We analysed the 2008 event because it provided a larger population of scars and lower errors in discharge estimation. We obtained the following mean height differences for each geomorphic form: 0.07 m in-channel (1 tree), 0.49 m in gravel bars (1 tree), 0.53 m in terrace 1 (3 trees), 0.26 m in terrace 2 (2 trees), 0.44 m in secondary channels of the cone (2 trees), 0.17 m in middle deposits of the cone (5 trees), 0.01 m in artificial levees (1 tree) and 0.63 m in right-side slopes (3 trees). The lowest variation in scar heights was observed inside the channel and on an artificial levee, but each of these geomorphic forms only contained one tree. If we consider geomorphic positions with more than a single tree, the lowest variation corresponded to trees located on terrace 2 or middle deposits of the cone, which are intermediate energy positions. The highest variation was observed on the right-side slope.

5. Discussion

5.1. Discussion of the results and new contributions

This paper presents a detailed multidisciplinary palaeoflood approach in an ungauged mountain stream (Portainé, Spanish Pyrenees) based on the four-topic correlation of geomorphology, dendrogeomorphology, flood discharge and flow hydrodynamics.

Detailed geomorphological mapping from total station data contributed to a good correlation between damaged trees and geomorphic forms. The formation of different dendrogeomorphological evidence

Table 3
Hydraulic parameters calculated for the specific location of the trees.

Tree				Hydraulic parameters		
Cross section	Bank location	Elevation	Scar date	Water depth (m)	Velocity (ms^{-1})	Unit stream power (Wm^{-2})
M-M′	Right	1029.42	2008	2.17	12.18	4542.02
K-K′	Channel	1019.13	2008	1.32	15.07	3291.31
Kb-Kb′	Channel	1015.45	2008	1.75	14.52	6403.48
Kc-Kc′	Right	1015.24	2008	0.96	6.15	1775.85
Kd-Kd′	Channel	1013.60	2008	1.43	14.02	5338.19
Ke-Ke′	Channel	1012.49	2008	1.21	13.55	3541.88
P-P′	Left	1008.98	2008	1.65	5.15	1899.26
O-O′	Channel	1007.51	2008	1.88	14.98	7375.25
O-O′	Left	1007.98	2010	1.48	6.02	1826.440
O-O′	Left	1007.98	2010	1.48	6.02	1826.440
Nb-Nb′	Right	1007.11	2008	1.22	4.37	362.72
Y-Y′	Left	995.25	2008	0.27	4.81	1365.61
Xb-Xb′	Left	993.14	2008	0.55	4.35	1294.98
Uc-Uc′	Left	985.80	2010	0.75	12.12	5476.54
Jb-Jb′	Left	978.70	2010	1.10	11.02	915.50
D-D′	Left	977.53	2008	1.12	9.08	592.94
F-F′	Left	976.75	2008	0.70	8.13	886.59
F-F′	Left	976.21	2008	1.24	8.13	886.59
C-C′	Left	975.75	2008	1.32	7.75	539.47
C-C′	Left	975.51	2008	1.56	7.75	539.47
G-G′	Left	975.19	2008	0.30	8.74	753.42
G-G′	Left	974.88	2008	0.61	8.74	753.42
A-A′	Left	973.75	2010	0.73	6.91	336.96
A-A′	Left	973.18	2010	1.30	6.91	336.96

(FDE) depends on the geomorphic location of the trees. Usually, the most energetic disturbances are found in trees located at energetic geomorphic forms (Ruiz-Villanueva et al., 2010). Nonetheless, in our study area, most FDE were found in geomorphic positions of intermediate energy. This is explained by: (i) the scarcity of trees on the riverbed (the most energetic positions) because high discharge events with significant stream power uproot and transport them, and (ii) the scarcity of external disturbances on the slopes (less energetic positions) due to the flow not having enough energy to produce damage on trees farther from the active channel, or the flow not even reaching those areas.

The estimation of peak discharges was possible thanks to the detailed cross sections measured in the field. LiDAR data were not accurate enough for the application of hydraulic models, due to the dense vegetation and therefore insufficient and inaccurate ground points. The method of palaeodischarge calculation for 2008 and 2010 was adapted from Ballesteros-Cánovas et al. (2010). Comparing the two years reconstructed, it seems that their magnitudes were similar; but the 2008 event has been reported as the most severe (IGC, 2013). This discrepancy could be explained by differences in the real pre-event topography, as we used the same topographic data for the hydraulic modelling in both cases, which includes boulder accumulation in the alluvial cone during extraordinary events. Therefore, the pre-2008 topography would have been lower than pre-2010, and the water stage for scar formation higher, leading to an underestimation of the 2008 event.

Table 5
Estimation of the mobilized particle size, obtained from equations proposed by different authors. Costa, Williams, Jacob and Gob et al.: intermediate axis of maximum boulders; Bagnold: intermediate axis of mode size (medium) boulders; Carling et al.: maximum axis of average size (medium) boulders.

Author	Equation	Numerical constants	Particle diameter (m)
Costa (1983)	Eq. (5)	a = 0.09 b = 1.686	2.62
Costa (1983) for coarse material	Eq. (5)	a = 0.03 b = 1.686	1.28
Williams (1983)	Eq. (5)	a = 0.079 b = 1.27	6.24
Jacob (2003)	Eq. (5)	a = 0.025 b = 1.647	1.70
Gob et al. (2003)	Eq. (5)	a = 0.0253 b = 1.62	1.91
Bagnold (1980), adapted by Ferguson (2005)	Eq. (6)	c_1 = 2860.5 c_2 = 12	1.63
Carling et al. (2002)	Eq. (7)	C_d = 0.95 *L-H-B* (field)	0.27

Critical overbank discharges calculated at the apex of the alluvial cone indicate the minimum discharge for the overflow of the left bank. However, this minimum discharge does not necessarily involve water flowing all along the cone, as it may return to the functional channel. In order to validate the estimations, we checked that the discharge, apart from overflowing the bank, showed water continuity along the distributary channels of the cone. Therefore, two overbank flow discharges were estimated: partial critical overbank discharge associated with levee breach and the formation of crevasse splays ($43\ m^3\ s^{-1}$), and total critical overbank discharge and cone flooding ($58\ m^3\ s^{-1}$).

Peak discharges for different return periods have been calculated for the Portainé basin by other authors using hydrologic modelling (De las Heras, 2016). Comparing those results with the palaeodischarge values obtained in this study for 2008 ($316\ m^3\ s^{-1}$) and 2010 ($314\ m^3\ s^{-1}$), both events would correspond to return periods of over 500 years. This makes no sense, as torrential or debris events have been recorded almost every year since 2006. Moreover, the critical overbank discharge obtained in the downstream part of the Portainé stream would correspond approximately to a 500-year return period. This means that: (i) the discharges estimated in this study may be overestimated; and (ii) the discharges with different return periods in De las Heras (2016) could be underestimated. In our study, this inconsistency could be due to the high sediment load not considered in the palaeohydrologic and palaeohydraulic analysis. As outlined by Bodoque et al. (2011), peak discharges are the result of the combination, not only the sum, of water and sediment load. This combination is very common in steep mountain streams with high torrential activity.

Table 4
Field measurements and relationships between the length (*L*), width (*B*) and height (*H*) of boulders accumulated in the alluvial cone.

Boulder number	Relative size	Length (m)	Width (m)	Height (m)	*B/L* ratio	*H/L* ratio
1	Large	0.67	0.48	0.3	0.72	0.45
2	Very large	1.52	0.88	0.92	0.58	0.61
3	Large	0.54	0.32	0.15	0.59	0.28
4	Medium	0.26	0.17	0.05	0.65	0.19
5	Medium	0.27	0.13	0.08	0.48	0.30
6	Small	0.17	0.15	0.08	0.88	0.47
7	Small	0.15	0.15	0.05	1.00	0.33
8	Very small	0.09	0.07	0.06	0.78	0.67
9	Medium	0.21	0.18	0.08	0.86	0.38
10	Medium	0.21	0.17	0.13	0.81	0.62
Average	Medium	0.29	0.21	0.12	0.74	0.43

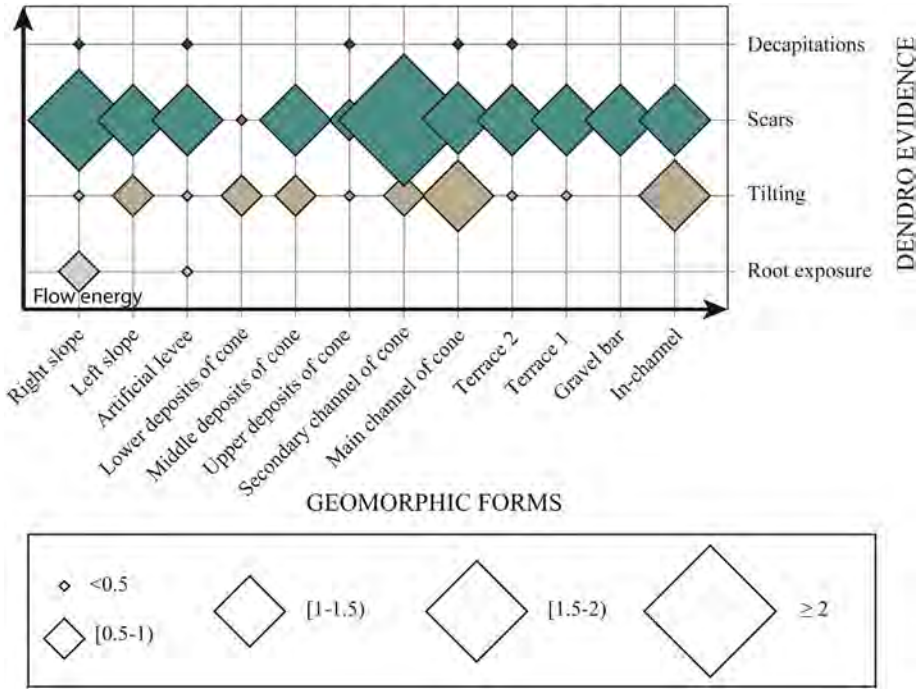

Fig. 8. Relation between dendrogeomorphological evidence and geomorphic forms, organized according to the increase of the flow energy. The size of the symbols represents the number of FDE per tree.

Regarding the calculation of the particle size transported by a specific flow, the best approach is that proposed by Carling et al. (2002), which we adapted for the study case. The resulting relation of maximum, medium and minimum boulder diameters is in agreement with the typology of the bedrock, which is composed of highly fractured metapelites. This leads to the formation of boulders with two similar axes and a considerably shorter one. However, the results obtained by Carling et al. (2002) correspond to the most common size of deposited boulders (medium size in the study area), as the relation between axis lengths was established for the average of the field measurements. Bagnold (1980) also considers the most common size, so the results are clearly overestimated. All the other authors produce equations to estimate the intermediate axis of the maximum transported boulder, so the results should be compared with the width of the largest boulders identified in the field (Table 4, boulder number 2). Among these equations, we consider that proposed by Costa (1983) for coarse material to be the most suitable in our case. In general, our results for the Portainé alluvial cone using empirical relations (Table 5) are larger than the boulder size measured in the field (Table 4). The causes of this could be that: (i) they are empirical relations calculated for biphasic flows exhibiting Newtonian behaviour, and some debris flows are uniphasic; (ii) the equations work with the mobilizable particle size, but boulders of that dimension are not always available to be moved on the river bottom, in part due to the lithology of the source area (even though this does not seem to occur in this case), or because they could be fragmented during the transport; (iii) stream power values are averaged for the channel or margins (using a 1D hydraulic model that only distinguishes three zones in each cross section), but they may not be representative of some specific positions; or (iv) the model works with Newtonian flows of clean water, so the calculated discharges may be overestimated due to the higher viscosity of the more dense real flow (which includes sediment), leading to an actual capacity to transport only smaller boulders. Considering these limitations, the results obtained by empirical relations are coherent with real torrential processes in the Portainé study area. The equation proposed by Williams (1983) is the exception and does not work for the stream studied.

The uncertainty in the peak discharge estimations depends on the reliability of scar heights (Ballesteros-Cánovas et al., 2016). The distribution of scar-flow differences in the study area suggests that trees located on the deposits of the cone and the terraces are the most suitable for palaeoflood reconstruction; while those standing in the slopes are less useful.

The present study is a new step in palaeoflood reconstruction in ungauged small basins. Even if the peak discharges obtained by our hydrodynamic modelling may be overestimated because we did not consider the sediment load, at least they allow us to estimate the order of magnitude of past events. Such a multidisciplinary approach could be very useful for basins where detailed dendrogeomorphological studies cannot be carried out (due to there being few or no riverbank trees) or the application of hydrologic–hydraulic models presents great limitations (due to there being scarce meteorological data or no accurate DEMs).

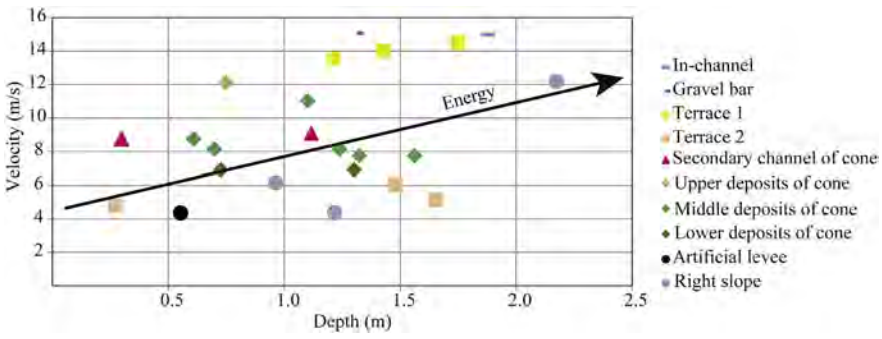

Fig. 9. Flow velocity–depth diagram for the formation of scars, classified by the geomorphic form in which they are located. The arrow indicates the increase of the flow energy.

5.2. Limitations of the data sources

The geomorphic positions of the trees could have changed over time, because the present-day landform, element or facet assigned to each tree may not be exactly the same as when the flood occurred and the scar was formed. This is certainly the case for geomorphic forms close to the river channel and especially for older dendrogeomorphological damage or FDE. This limitation of the data source is very difficult to remedy, due to the lack of previous geomorphological maps or detailed aerial photographs.

Scars were used as PSIs, considering that their maximum height indicates the minimum water table of the flow and is close to high water marks (HWM). Nevertheless, this approximation involves some uncertainties and error sources: (i) PSIs can be higher than HWM if the scar was formed by material accumulated upstream from a tree, leading to discharge overestimation (Ballesteros-Cánovas et al., 2010); (ii) PSIs can be lower than HWM when the scar is partially closed and therefore the discharge would be underestimated (Guardiola-Albert et al., 2015); and (iii) PSIs can be lower than HWM when the scar has been produced by the sediment load in the lower part of the water column (bedload transport, *e.g.* saltation), and not by the impact of floating load (large pieces of wood), so the discharge may be underestimated (Ballesteros-Cánovas et al., 2010). The trial-and-error technique was applied to compare the height of the PSIs (height of the scars) and the water stage modelled in each cross section (Yanosky and Jarrett, 2002). Despite the small number of trees, we had multiple scars to simulate the flow of the 2008 (18 scars) and 2010 events (6 scars). Moreover, the existing technical reports of the 2008 and 2010 events (IGC, 2010a, 2010b), especially upstream, seem to be in agreement with our results for the magnitude of these events.

The topographic data presented the following drawbacks: (i) there was a temporal difference between the detailed field topography (2014) and airborne LiDAR data (2011); (ii) we used the same DEM for hydrodynamic modelling of different years; and (iii) LiDAR data have a low degree of accuracy in forested or densely vegetated areas. Temporal changes of the terrain in the alluvial cone indicate that the scars on trees located upstream of this area are more reliable for palaeoflood discharge estimations, but they are scarcer. So, the main topographic limitations were overcome by acquiring highly accurate data for multiple cross sections, coinciding with the location of the damaged trees.

5.3. Limitations of the methods

Tree-ring analysis is very useful when acquiring data on past flood events (Ballesteros-Cánovas et al., 2015b; Stoffel and Bollschweiler, 2008). However, dendrogeomorphological methodologies present some drawbacks (Díez-Herrero et al., 2013). In our study area, (i) some FDE could correspond to different events that occurred in a same year (at least two in 2008 and another two in 2010), and therefore, the FDE from the same year could correspond to different intra-annual events; (ii) scars can be produced by other external factors that are not related to torrential processes, like the impact of a falling tree during storms or human activity. However, in this study, the position, shape, orientation and distribution of the scars were analysed in detail with regard to their relation to torrential processes, and the doubtful ones were dismissed.

The hydrodynamic modelling was carried out with the HEC-RAS 1D hydraulic model (USACE, 2008) that works with transversal cross sections. The area between them is lineally interpolated and may involve some errors. This was minimized by acquiring detailed topographic data with a total station in the field and, in a few cases, introducing additional sections corresponding to the position of trees showing scars from the 2008 or 2010 events. A 2D model was not run, due to geometric, hydrodynamic and other factors (see Section 3.3.). Moreover, other work, such as Bodoque et al. (2011), uses 1D hydraulic modelling for peak discharge reconstruction in steep-gradient mountain reaches showing the same configuration and characteristics as the Portainé stream, supporting its suitability. The small differences in peak discharges obtained from the TIN-based cross sections and the field-based cross sections can be explained by the longitudinal variation of the high sediment load flow and the different number of scars in each case.

5.4. Limitations of the results

Our flow hydraulics results were not contrasted with real data, because of the lack of flow gauging stations within the basin. Therefore, the palaeodischarges could not be compared and validated with actual records. Nevertheless, the discharges obtained in this study seem reasonable, and their order of magnitude is coherent with the dimensions of the river and the catchment.

5.5. Further research

Future steps that could improve the characterization of the Portainé stream and palaeoflood reconstruction are: (i) the integration of the sediment load and transport, which constitute important factors for the rheology of torrential and debris floods; (ii) the use of 2D hydrodynamic modelling, to simulate the limited transversal flows and therefore secondary discharges along the alluvial cone.

Last but not least, the methodology adopted in this study could be applied to other watersheds of similar morphometric and geomorphologic characteristics. The validation of the use of 1D hydraulic models in other small elongated cones in mountainous areas with few source data and relatively few trees would corroborate the strong potential of such multidisciplinary analysis for problematic torrential settings.

6. Conclusions

The palaeohydrological approach presented in this study proves that the flow energy obtained from hydrodynamic modelling of past events, determined by depth, velocity and stream power, shows a positive correlation with most energetic geomorphic forms (riverbed and low alluvial terraces). However, most of the external disturbances are found on trees located in geomorphic positions of intermediate energy (the alluvial cone). Trees showing less uncertainty for hydraulic modelling, based on the variation in scar heights, were also located at geomorphic forms formed by intermediate energy processes (high alluvial terraces and deposits of the cone). These findings suggest that the most reliable scarred trees for peak discharge estimations using hydraulic modelling correspond to intermediate-energy flow positions.

The present work shows the potential of the combination of techniques for flood assessment in problematic contexts, such as ungauged mountain basins or where hydrological data are scarce, densely vegetated areas with poor topographic data, and rivers with few disturbed trees for detailed dendrogeomorphological studies.

Supplementary data to this article can be found online at https://doi.org/10.1016/j.catena.2017.11.009.

Acknowledgements

This work was funded by the CHARMA project (CGL2013-40828-R) of the Spanish Ministry of Economy, Industry and Competitiveness (MINEICO) and by a PhD studentship of the lead author (APIF 2014-2015) paid by the University of Barcelona (UB). The authors thank Dr. Mar Tapia for her advice on statistical analysis. We are also grateful for comments from three anonymous reviewers which improved the manuscript.

References

Arcement, G.J., Schneider, V.R., 1989. Guide for Selecting Manning's Roughness Coefficients for Natural Channels and Flood Plains, United States Geological Survey Water-Supply Paper 2339.

Bagnold, R.A., 1980. An empirical correlation of bedload transport rate in flumes and natural rivers. Proc. R. Soc. Lond. 372, 453–473. http://dx.doi.org/10.1098/rspa.1983.0054.

Baker, V.R., 1987. Paleoflood hydrology and extraordinary flood events. J. Hydrol. 96, 79–99. http://dx.doi.org/10.1016/0022-1694(87)90145-4.

Baker, V.R., 2008. Paleoflood hydrology: Origin, progress, prospects. Geomorphology 101, 1–13. http://dx.doi.org/10.1016/j.geomorph.2008.05.016.

Baker, V.R., Pickup, G., 1987. Flood geomorphology of the Katherine Gorge, Northern Territory, Australia. Geol. Soc. Am. Bull. 98, 635–646. http://dx.doi.org/10.1130/0016-7606(1987)98<635:FGOTKG>2.0.CO;2.

Baker, V.R., Kochel, R.C., Patton, P.C., 1988. Flood Geomorphology. John Wiley and Sons, New York, United States (ISBN: 978-0-12-394846-5).

Ballesteros-Cánovas, J.A., Eguibar, M.Á., Bodoque, J.M., Díez-Herrero, A., Stoffel, M., Gutiérrez-Pérez, I., 2010. Estimating flash flood discharge in an ungauged mountain catchment with 2D hydraulic models and dendrogeomorphic palaeostage indicators. Hydrol. Process. 25, 970–979. http://dx.doi.org/10.1002/hyp.7888.

Ballesteros-Cánovas, J.A., Márquez-Peñaranda, J.F., Sánchez-Silva, M., Díez-Herrero, A., Ruiz-Villanueva, V., Bodoque, J.M., Eguibar, M.Á., Stoffel, M., 2015a. Can tree tilting be used for paleoflood discharge estimations? J. Hydrol. 529, 480–489. http://dx.doi.org/10.1016/j.jhydrol.2014.10.026.

Ballesteros-Cánovas, J.A., Stoffel, M., St George, S., Hirschboeck, K., 2015b. A review of flood records from tree rings. Prog. Phys. Geogr. 29 (6), 1–23. http://dx.doi.org/10.1177/0309133315608758.

Ballesteros-Cánovas, J.A., Stoffel, M., Spyt, B., Janecka, K., Kaczka, R.J., Lempa, M., 2016. Paleoflood discharge reconstruction in Tatra Mountain streams. Geomorphology 272, 92–101. http://dx.doi.org/10.1016/j.geomorph.2015.12.004.

Barredo, J.I., 2007. Major flood disasters in Europe: 1950–2005. Nat. Hazards 42, 125–148. http://dx.doi.org/10.1007/s11069-006-9065-2.

Benito, G., Díez-Herrero, A., 2015. Palaeoflood hydrology: reconstructing rare events and extreme flood discharges. In: Shroder, J.F., Paron, P., Di Baldassarre, G. (Eds.), Hydro-meteorological Hazards, Risks, and Disasters. Elsevier, Amsterdam, The Netherlands, pp. 65–104 (ISBN: 978-0-12-394846-5).

Benito, G., Sopeña, A., Sánchez-Moya, Y., Machado, M.J., Pérez-González, A., 2003. Palaeoflood record of the Tagus River (Central Spain) during the Late Pleistocene and Holocene. Quat. Sci. Rev. 22, 1737–1756. http://dx.doi.org/10.1016/S0277-3791(03)00133-1.

Benito, G., Macklin, M.G., Zielhofer, C., Jones, A.F., Machado, M.J., 2015. Holocene flooding and climate change in the Mediterranean. Catena 130, 13–33. http://dx.doi.org/10.1016/j.catena.2014.11.014.

Bodoque, J.M., Eguibar, M.Á., Díez-Herrero, A., Gutiérrez-Pérez, I., Ruiz-Villanueva, V., 2011. Can the discharge of a hyperconcentrated flow be estimated from paleoflood evidence? Water Resour. Res. 47, 1–14. http://dx.doi.org/10.1029/2011WR010380.

Carling, P.A., Hoffmann, M., Blatter, A.S., Webb, R.H., 2002. Initial motion of boulders in bedrock channels. In: House, P.K., Baker, V.R., Levish, D.R. (Eds.), Ancient Floods, Modern Hazards: Principles and Applications of Paleoflood Hydrology. American Geophysical Union, Washington, DC, United States, pp. 147–160. http://dx.doi.org/10.1029/WS005p0147.

Chanson, H., 2004. Environmental Hydraulics of Open Channel Flows. Elsevier, Oxford, United Kingdom (ISBN: 978-0-7506-6165-2).

Chow, V.T., 1959. Open Channel Hydraulics. McGraw-Hill, New York, United States (ISBN: 07-010776-9).

Church, M., Biron, P., Roy, A., 2012. Gravel Bed Rivers: Processes, Tools, Environments. Wiley-Blackwell, Chichester, United Kingdom (ISBN: 978-0-470-68890-8).

Cook, E.R., Kairiukstis, L.A., 1990. Methods of Dendrochronology. Applications in the Environmental Sciences. Springer, Dordrecht, Netherlands. http://dx.doi.org/10.1007/978-94-015-7879-0.

Costa, J.E., 1983. Paleohydraulic reconstruction of flash-flood peaks from boulder deposits in the Colorado Front Range. Geol. Soc. Am. Bull. 94, 986–1004. http://dx.doi.org/10.1130/0016-7606(1983)94<986:profpf>2.0.co;2.

De las Heras, Á., 2016. Modificación de la respuesta hidrológica en avenidas torrenciales ante los cambios de usos del suelo en una cuenca de montaña (Portainé, Pirineo leridano). Archivo Digital UPM, Spain available at: http://oa.upm.es/45430/.

Díez-Herrero, A., 2015. Buscando riadas en los árboles: dendrogeomorfología. Enseñanza las Ciencias la Tierra 23 (3), 272–285 (ISSN: 1132-9157).

Díez-Herrero, A., Ballesteros-Cánovas, J.A., Bodoque, J.M., Ruiz-Villanueva, V., 2013. A new methodological protocol for the use of dendrogeomorphological data in flood risk analysis. Hydrol. Res. 44 (2), 234–247. http://dx.doi.org/10.2166/Nh.2012.154.

ESRI, 2014. ArcGIS 10.2.2 Desktop. Environmental Systems Research Institute, Redlands, United States.

Ferguson, R.I., 2005. Estimating critical stream power for bedload transport calculations in gravel-bed rivers. Geomorphology 70, 33–41. http://dx.doi.org/10.1016/j.geomorph.2005.03.009.

Furdada, G., Génova, M., Guinau, M., Victoriano, A., Khazaradze, G., Díez-Herrero, A., Calvet, J., 2016. Las avenidas torrenciales de los barrancos de Portainé, Reguerals y Ramiosa (Pirineo Central): evolución de las cuencas y dinámica torrencial. In: Durán Valsero, J.J., Montes Santiago, M., Robador Moreno, A., Salazar Rincón, Á. (Eds.), Comprendiendo El Relieve: Del Pasado Al Futuro. Instituto Geológico y Minero de España, Madrid, Spain, pp. 315–322 (ISBN: 978-84-9138-013-9).

García-Oteyza, J., Génova, M., Calvet, J., Furdada, G., Guinau, M., Díez-Herrero, A., 2015. Datación de avenidas torrenciales y flujos de derrubios mediante metodologías dendrogeomorfológicas (barranco de Portainé, Lleida, España). Ecosistemas 24, 43–50. http://dx.doi.org/10.7818/ECOS.2015.24-2.07.

Gaume, E., Bain, V., Bernardara, P., Newinger, O., Barbuc, M., Bateman, A., Blaškovičová, L., Blöschl, G., Borga, M., Dumitrescu, A., Daliakopoulos, I., Garcia, J., Irimescu, A., Kohnova, S., Koutroulis, A., Marchi, L., Matreata, S., Medina, V., Preciso, E., Sempere-Torres, D., Stancalie, G., Szolgay, J., Tsanis, I., Velasco, D., Viglione, A., 2009. A compilation of data on European flash floods. J. Hydrol. 367, 70–78. http://dx.doi.org/10.1016/j.jhydrol.2008.12.028.

Génova, M., Máyer, P., Ballesteros-Cánovas, J.C., Rubiales, J.M., Saz, M.A., Díez-Herrero, A., 2015. Multidisciplinary study of flash floods in the Caldera de Taburiente National Park (Canary Islands, Spain). Catena 131, 22–34. http://dx.doi.org/10.1016/j.catena.2015.03.007.

Gob, F., Petit, F., Bravard, J.P., Ozer, A., Gob, A., 2003. Lichenometric application to historical and subrecent dynamics and sediment transport of a Corsican stream (Figarella River - France). Quat. Sci. Rev. 22, 2111–2124. http://dx.doi.org/10.1016/S0277-3791(03)00142-2.

Gottesfeld, A.S., 1996. British Columbia flood scars: maximum flood stage indicators. Geomorphology 14, 319–325. http://dx.doi.org/10.1016/0169-555X(95)00045-7.

Grissino-Mayer, H.D., 2001. Evaluating crossdating accuracy: a manual and tutorial for the computer program COFECHA. Tree Ring Res. 57 (2), 205–221.

Guardiola-Albert, A., Ballesteros-Cánovas, J.A., Stoffel, M., Díez-Herrero, A., 2015. How to improve dendrogeomorphic sampling: variogram analyses of wood density using XRCT. Tree Ring Res. 71 (1), 25–36. http://dx.doi.org/10.3959/1536-1098-71.1.25.

IGC, 2010a. Estudi de la torrentada de la nit del dia 11 al 12 de setembre de 2008 al barranc de Portainé (Pallars Sobirà), AP-019/10. Institut Geològic de Catalunya, Barcelona, Spain.

IGC, 2010b. Nota de la visita al barranc de Portainé (Pallars Sobirà) arran del episodi de pluges dels dies 22 i 23 de juliol de 2010, AP-046/10. Institut Geològic de Catalunya, Barcelona, Spain.

IGC, 2013. Avaluació de la dinàmica torrencial del torrent de Portainé, AP-035/13. Institut Geològic de Catalunya, Barcelona, Spain.

Jacob, N., 2003. Les vallées en gorges de la Cévenne vivaraise: montagne de sable et château d'eau (PhD dissertation). Université Paris-Sorbonne, France.

Keim, R.F., Skaugset, A.E., Bateman, D.S., 1999. Digital terrain modeling of small stream channels with a total-station theodolite. Adv. Water Resour. 23, 41–48. http://dx.doi.org/10.1016/S0309-1708(99)00007-X.

Khazaradze, G., Guinau, M., Calvet, J., Furdada, G., Victoriano, A., Génova, M., 2016. Debris flow cartography using differential GNSS and Theodolite measurements. Geophys. Res. Abstr. 18, 9696. http://dx.doi.org/10.13140/RG.2.2.27245.59363.

Kochel, R.C., Baker, V.R., 1982. Paleoflood Hydrology. Science 215, 353–361. http://dx.doi.org/10.1126/science.215.4531.353.

Kundzewicz, Z., Stoffel, M., Kaczka, R., Wyżga, B., Niedźwiedź, T., Pińskwar, I., Ruiz-Villanueva, V., Łupikasza, E., Czajka, B., Ballesteros-Cánovas, J., Małarzewski, Ł., Choryński, A., Janecka, A., Mikuś, P., 2014. Floods at the northern foothills of the Tatra Mountains-a Polish–Swiss research project. Acta Geophys. 62 (3), 620–641. http://dx.doi.org/10.2478/s11600-013-0192-3.

Lang, M., Fernandez-Bono, J.F., Recking, A., Naulet, R., Grau-Gimeno, P., 2004. Methodological guide for paleoflood and historical peak discharge estimation. In: Benito, G., Thorndycraft, V.R. (Eds.), Systematic, Palaeoflood and Historical Data for the Improvement of Flood Risk Estimation: Methodological Guidelines. CSIC, Madrid, Spain, pp. 43–53 (ISBN:84-921958-3-5).

Luis-Fonseca, R., Raïmat, C., Hürlimann, M., Abancó, C., Moya, J., Fernández, J., 2011. Debris-flow protection in recurrent areas of the Pyrenees. Experience of the VX systems from output results collected in the pioneer monitoring station in Spain. In: 5th International Conference on Debris-Flow Hazards Mitigation, Padua, Italy, pp. 1063–1071.

Malik, I., Matyja, M., 2008. Bank erosion history of a mountain stream determined by means of anatomical changes in exposed tree roots over the last 100 years (Bila Opava River–Czech Republic). Geomorphology 98, 126–142. http://dx.doi.org/10.1016/j.geomorph.2007.02.030.

Meteocat, 2008. Atles Climàtic de Catalunya 1961–1990. Servei Meteorològic de Catalunya, Barcelona, Spain.

Nicholas, A.P., Walling, D.E., 1997. Modelling flood hydraulics and overbank deposition on river floodplains. Earth Surf. Process. Landf. 22, 59–77. http://dx.doi.org/10.1002/(SICI)1096-9837(199701)22:1<59::AID-ESP652>3.0.CO;2-R.

O'Connor, J.E., Webb, R.H., 1988. Hydraulic modelling for paleoflood analysis. In: Baker, V.C., Kochel, R.C., Patton, P.C. (Eds.), Flood Geomorphology. John Wiley & Sons, New York, United States, 978-0-471-62558-2, pp. 393–402.

Ortega, J.A., Garzón, G., 1997. Inundaciones históricas en el rio Guadiana: sus implicaciones climáticas. In: Rodríguez, J. (Ed.), Cuaternario Ibérico. AEQUA, Huelva, Spain, pp. 365–367.

Palau, R.M., Hürlimann, M., Pinyol, J., Moya, J., Victoriano, A., Génova, M., Puig-Polo, C., 2017. Recent debris flows in the Portainé catchment (Eastern Pyrenees, Spain): analysis of monitoring and field data focussing on the 2015 event. Landslides 14, 1161–1170. http://dx.doi.org/10.1007/s10346-017-0832-9.

Portilla, M., Chevalier, G., Hürlimann, M., 2010. Description and analysis of the debris flows occurred during 2008 in the Eastern Pyrenees. Nat. Hazards Earth Syst. Sci. 10, 1635–1645. http://dx.doi.org/10.5194/nhess-10-1635-2010.

RinnTech, 2003. TSAP-Win Software for Tree-ring Measurement, Analysis and Presentation Product Information, v. 0.53. RinnTech, Heidelberg, Germany (2 pp.).

Ruiz-Villanueva, V., Díez-Herrero, A., Stoffel, M., Bollschweiler, M., Bodoque, J.M., Ballesteros, J.A., 2010. Dendrogeomorphic analysis of flash floods in a small ungauged mountain catchment (Central Spain). Geomorphology 118, 383–392. http://dx.doi.org/10.1016/j.geomorph.2010.02.006.

Sánchez-Moya, Y., Sopeña, A., 2015. Aprendiendo a leer en las estratificaciones cruzadas. Enseñanza las Ciencias la Tierra 23 (2), 148–159 (ISNN: 1132-9157).

Sigafoos, R.S., 1964. Botanical evidence of floods and flood-plain deposition. In: United States Geological Survey Professional Paper 485-A.
Stoffel, M., Bollschweiler, M., 2008. Tree-ring analysis in natural hazards research - an overview. Nat. Hazards Earth Syst. Sci. 8, 187–202. http://dx.doi.org/10.5194/nhess-8-187-2008.
Stoffel, M., Corona, C., 2014. Dendroecological dating of geomorphic disturbance in trees. Tree Ring Res. 70 (1), 3–20. http://dx.doi.org/10.3959/1536-1098-70.1.3.
Tarolli, P., 2014. High-resolution topography for understanding Earth surface processes: Opportunities and challenges. Geomorphology 216, 295–312. http://dx.doi.org/10.1016/j.geomorph.2014.03.008.
Terrasolid, 2016. TerraScan User's Guide. Terrasolid Ltd., Helsinki, Finland (592 pp.).
USACE, 2008. HEC-RAS River Analysis System Users's Manual, v. 4.0. Hydrologic Engineering Center, Washington, DC, United States (747 pp.).
USACE, 2012. HEC-GeoRAS GIS Tools for Support of HEC-RAS using ArcGIS 10 User's Manual, v. 10. Hydrologic Engineering Center, Washington, DC, United States (242 pp.).
Victoriano, A., Guinau, M., Furdada, G., Calvet, J., Cabré, M., Moysset, M., 2016. Aplicación de datos LiDAR en el estudio de la dinámica torrencial y evolución de los barrancos de Portainé y Reguerals (Pirineos Centrales). In: Durán Valsero, J.J., Montes Santiago, M., Robador Moreno, A., Salazar Rincón, Á. (Eds.), Comprendiendo El Relieve: Del Pasado Al Futuro. Instituto Geológico y Minero de España, Madrid, pp. 447–455 (ISBN:978-84-9138-013-9).
Webb, R.H., Jarrett, R.D., 2002. One-dimensional estimation techniques for discharges of paleofloods and historical floods. In: House, P.K., Webb, R.H., Baker, V.R., Levish, D.R. (Eds.), Ancient Floods, Modern Hazards: Principles and Applications of Paleoflood Hydrology. American Geophysical Union, Washington, DC, pp. 111–125. http://dx.doi.org/10.1029/WS005p0111.
Williams, G.P., 1983. Paleohydrological methods and some examples from Swedish fluvial environments. Geogr. Ann. 65, 227–243. http://dx.doi.org/10.2307/520588.
Yanosky, T.M., Jarrett, R.D., 2002. Dendrochronologic evidence for the frequency and magnitude of paleofloods. In: House, P.K., Webb, R.H., Baker, V.R., Levish, D.R. (Eds.), Ancient Floods, Modern Hazards: Principles and Applications of Paleoflood Hydrology. American Geophysical Union, Washington, DC, pp. 77–89. http://dx.doi.org/10.1029/WS005p0077.
Zielonka, T., Holeksa, J., Ciapala, S., 2008. A reconstruction of flood events using scarred trees in the Tatra Mountains, Poland. Dendrochronologia 26, 173–183. http://dx.doi.org/10.1016/j.dendro.2008.06.003.